

Optical Center Estimation for Lenslet-based Plenoptic Cameras

Wei Hu
Peking University
Beijing, China
forhuwei@pku.edu.cn

Mozhdeh Seifi
Technicolor
Rennes, France
mozhde.seifi@gmail.com

Erik Reinhard
Technicolor
Rennes, France
erik.reinhard@technicolor.com

Abstract—Plenoptic cameras enable a variety of novel post-processing applications, including refocusing and single-shot 3D imaging. To achieve high accuracy, such applications typically require knowledge of intrinsic camera parameters. One such parameter is the location of the main lens’ optical center relative to the sensor, which is required for modeling radially symmetric optical effects. We show that estimating this parameter can be achieved to an accuracy of less than half a pixel by utilising the symmetry inherent in each micro-image. Further, we show that estimating this parameter separately allows all other intrinsic camera parameters to be estimated with higher accuracy than can be achieved using a single optimization scheme, and leads to better vignetting correction than with an inaccurate optical center.

I. INTRODUCTION

Plenoptic cameras capture spatio-angular information of the light field [1], enabling post-processing applications such as refocusing [1], depth estimation [2] and 3D imaging from a single shot [3]. This is achieved by placing a microlens array between the main lens and the imaging sensor. Each microlens focuses bundles of light with different angles of incidence onto different pixels, creating a micro-image on the sensor.

This technology, while still relatively immature today, is gaining importance as time goes. Early indications are the arrival of the Lytro cinema¹, movements in standardization bodies such as H.264/MPEG-4 AVC [4], the MPEG call for light field test materials [5], and JPEG Pleno², as well as ever increasing pixel resolutions in display devices that will eventually lead to glasses-free 3D. With maturing light field technologies, enhancing the accuracy of acquisition systems is an important area of research. In particular, post-processing applications often require fundamental image formation modeling that describes the light transport within a camera [6]. Such models require knowledge of intrinsic camera parameters, including the focal length of the main lens and that of the microlenses. One parameter is the point at which the optical axis of the main lens intersects the sensor plane, known as the optical center. It determines the characteristics of several radially symmetric image properties, such as vignetting [7],

radial lens distortion and field curvature. An accurate estimate of the optical center would help any techniques aimed at correcting for these effects. In addition, the optical center could play a role in novel light field applications such as light field stitching. Here, camera rotations around the optical center would be used to increase the size of the acquired light field [8].

Further, the estimation of intrinsic camera parameters is normally achieved through optimization schemes. Their accuracy and speed of convergence depend on the number of parameters to be optimized. We show that their accuracy may be improved by separately calculating the optical center using our proposed technique, leaving an optimization problem with fewer parameters.

The optical center is rarely specified by camera manufacturers, and may vary between cameras (even of the same brand and type). While it is not studied for plenoptic cameras, the deviation of the optical center from the center of the sensor in conventional cameras may reach as many as 40 pixels [9]. Further, the optical center may also vary with respect to focal length and zoom settings. Hence, optical center estimation would be necessary under different camera parameter settings. Such characterization can be used both as a tool in the design process of plenoptic cameras, as well as a tool for the characterization of existing systems to make the aforementioned light-field processing and editing tasks more accurate.

For conventional cameras, optical center estimation typically follows one of two approaches. The first directly calibrates the optical center via a general camera calibration procedure [10], [11], [12]. The second estimates the optical center by measuring vignetting [9] or radial lens distortion [13]. However, due to the presence of a microlens array, image formation in plenoptic cameras does not admit a similar analysis, making the second category of techniques inappropriate for plenoptic camera calibration. To the best of our knowledge, there is currently no other work on optical center estimation tailored for plenoptic cameras.

To address this problem, we propose an accurate and robust approach to estimate the optical center of plenoptic cameras, based on the observation that when a uniform surface is imaged by a plenoptic camera, each micro-image exhibits relatively strong vignetting which is reflection symmetric

¹<https://www.lytro.com/cinema>

²<https://jpeg.org/jpegpleno/>

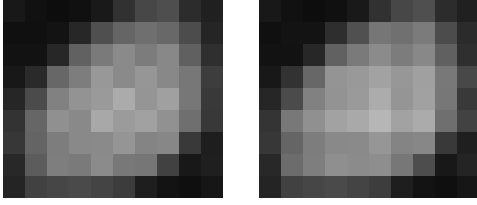


Fig. 1. A micro-image in a raw white image (left), and the same micro-image after demosaicking (right).

relative to an axis that intersects the optical center. As an example, Fig. 1 shows a micro-image of a white surface (i.e. a *white image*) before (left) and after demosaicking (right). As can be seen, a white surface imaged through a single microlens forms an approximately elliptical shape with its luminance attenuated due to vignetting of the main lens (a.k.a. cat’s eye vignetting) [6]. The minor axis of the ellipse intersects the optical center of the main lens.

There exist several symmetry detection algorithms that can in principle be applied to the pixels of each micro-image. A requirement of a suitable symmetry detection algorithm is to maintain sufficient accuracy, despite the small size of typical micro-images. Note, for instance, that the first generation Lytro camera contains micro-images that are no larger than 10×10 pixels. The presence of noise means that using such a small number of pixels to detect symmetry can lead to limited reliability.

Existing symmetry detection algorithms are based on histogram of gradient orientations [14], on multi-resolution morphological operators [15], or on learning based techniques [16]. Although the first two approaches perform well in the general case, micro-images are typically too small to allow reliable results, while learning-based techniques tend to be computationally expensive.

To improve robustness, we have found that rather than analysing pixels individually (or in pairs) to determine symmetry, there is advantage in analysing pairs of small patches of pixels. In particular, the dominant gradient directions of patches may be analysed, and these can be conveniently represented by structure tensors [17].

The analysis of each micro-image leads to a separate independent estimation of a line that intersects with the camera’s optical center. The optical center can therefore be estimated as the intersection point of all these lines, which in presence of noise is estimated as the point that is the closest to all of these lines.

Our approach yields an accuracy one to two orders of magnitude higher than what can currently be achieved for conventional cameras, which we attribute in part to our algorithm design and in part to better information available in plenoptic imagery. We evaluate two brands of plenoptic cameras, and show that their optical centers have statistically significant deviation from the center of the sensor. Finally, we show that separating the optical center estimation from the calculation of the remaining intrinsic camera parameters improves the

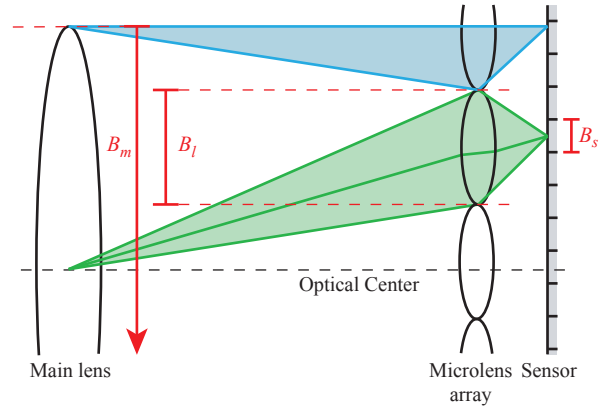


Fig. 2. Light transport in a general microlens-based plenoptic camera. Only the top-half is shown. The masking functions for modeling main lens and microlens aperture occlusions are marked in red.

accuracy of all parameters, and leads to better vignetting correction than initializing with an inaccurate optical center.

II. MICRO-IMAGE SYMMETRY

Reflection symmetry in micro-images originates from light transport within the optical system of a plenoptic camera. When bundles of light rays propagate through a microlens-based plenoptic camera, some are occluded by the aperture of the main lens, while others are refracted by the main lens and propagate to the microlens array, as shown in Fig. 2. These ray bundles are then either occluded or refracted by microlenses. Ray bundles that arrive at the sensor will be integrated and sampled to form pixels.

While micro-images are reflection symmetric by observation, we can also analyze the nature of the micro-image symmetry from an appropriate computational model of such light transport [6]. According to [6], the pixel intensity is nonzero only if light passes through two circular masks, which are normally spatially offset w.r.t. each other. Fig. 2 demonstrates two such cases: the lower pixel shows a full overlap of the two disks, i.e., its intensity is the integral over ray bundles that pass through the main lens and the entire corresponding microlens. The upper pixel shows a partial overlap, so that some rays are occluded by the main lens. This partial overlap leads to a phenomenon known as cat’s eyes, which increases with distance to the optical center. This is the cause for reflection symmetry in micro-images, which is oriented along the line connecting the centers of the two disks [18].

As the centers of the two circular masks are the projected centers of the main lens and the corresponding microlens on the sensor [6], we derive that *in a uniform image captured by a plenoptic camera, each micro-image is reflection symmetric in terms of pixel intensity w.r.t. a line that passes through the optical center and the corresponding microlens center*. This motivates us to determine the optical center by estimating the intersection point of the symmetry axes, which will be discussed in the next section.

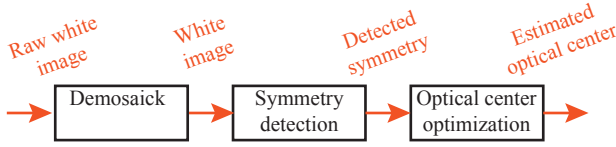


Fig. 3. Overview of our optical center estimation algorithm.

III. ALGORITHM

An overview of the proposed optical center estimation algorithm is shown in Fig. 3. The input consists of a raw image taken with a plenoptic camera of a white scene (the white image), which is subsequently demosaicked [19].

The symmetry axis $\hat{\mathbf{a}}$ of each micro-image \mathbf{I} is estimated as the one that maximizes the number of symmetric point pairs in that micro-image. We consider two points symmetric w.r.t. a line when their predominant gradient orientations are symmetric. Here the predominant gradient orientation of a point is computed from the structure tensor [17] of a patch centered at that point. We have chosen this particular approach as it is more robust to noise than either comparing intensities directly, or analyzing finite differences. Note that each micro-image could be analyzed independently and in parallel. Details of this step are given in Section III-A.

For each micro-image an axis of symmetry is estimated. We then estimate the optical center as the point that has the smallest total distance to all the detected symmetry axes. Section III-B describes this step in detail.

A. Symmetry Detection

We first define the symmetry axis $\mathbf{a} = (a_1, a_2, a_3)$ of a micro-image \mathbf{I} as the line $\mathbf{a} \cdot (x, y, 1)^T = 0$ that maximizes the number of symmetric point pairs in \mathbf{I} , and additionally has a valid orientation. Validity is established by requiring that the distance of the line \mathbf{a} to the center of the sensor \mathbf{c}_s remains below a given threshold t . This requirement is based on the observation that in good optical designs, the optical center is not arbitrarily far removed from the center of the sensor.

To estimate a symmetry axis, an optimization scheme may be employed, whereby for each candidate axis the level of symmetry is evaluated. Such evaluation proceeds by taking for each pixel $\mathbf{p} = (p_1, p_2)$ in the micro-image its corresponding reflection symmetric point \mathbf{q} , which can be calculated as follows:

$$\mathbf{q} = \mathbf{p} - \frac{2\mathbf{a} \cdot (p_1, p_2, 1)^T}{a_1^2 + a_2^2} \begin{bmatrix} a_1 \\ a_2 \end{bmatrix}. \quad (1)$$

This makes \mathbf{a} the perpendicular bisector of the line segment connecting \mathbf{p} and \mathbf{q} . We refer to \mathbf{p} and \mathbf{q} as corresponding points hereafter. If certain features of pixels \mathbf{p} and \mathbf{q} are similar, then this point pair can be thought of as contributing a vote toward establishing candidate axis \mathbf{a} as a good estimate of the reflection symmetry in micro-image \mathbf{I} .

We introduce the function $g(\cdot)$ to calculate robust features of pixels \mathbf{p} and \mathbf{q} . It determines which attribute of a point we require to be symmetric. For instance, we could define $g(\mathbf{p})$

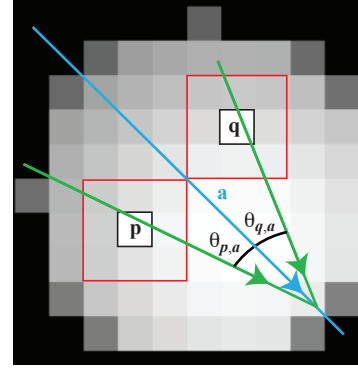


Fig. 4. Symmetry detection for a point pair (\mathbf{p}, \mathbf{q}) by comparing the angles between a candidate line \mathbf{a} (marked in blue) and predominant gradient directions (marked in green) of the corresponding pixel patches (marked in red).

to be the pixel intensity according to Property 1. However, this feature would not lead to robust results in the presence of noise. A similar argument could be made for directly using pixel gradients.

Instead, we propose to determine the symmetry of each point pair (\mathbf{p}, \mathbf{q}) w.r.t. \mathbf{a} by comparing the predominant gradient directions of two pixel patches of size $m \times m$ ($m \in \mathbb{N}$) centered at \mathbf{p} and \mathbf{q} , respectively. We set $m = 3$ in our experiments. The predominant gradient directions of a pixel can be robustly estimated by its structure tensor. It is a positive semi-definite second-moment matrix of the image gradient, and is defined as:

$$\mathbf{T} = \begin{bmatrix} \bar{I}_x^2 & \bar{I}_x \bar{I}_y \\ \bar{I}_y \bar{I}_x & \bar{I}_y^2 \end{bmatrix}, \quad (2)$$

where \bar{I}_x and \bar{I}_y are the partial derivatives of a pixel patch $\bar{\mathbf{I}}$ in the horizontal and vertical directions, respectively. The partial derivatives \bar{I}_x and \bar{I}_y are calculated using Gaussian derivative filters [17].

Eigen decomposition is then applied to \mathbf{T} to acquire eigenvalues $\{\alpha_1, \alpha_2\}$ (sorted such that $\alpha_1 \geq \alpha_2$) and the corresponding orthonormal eigenvectors $\{\mathbf{v}_1, \mathbf{v}_2\}$. If $\alpha_1 > \alpha_2$, then \mathbf{v}_1 gives the predominant gradient direction. If $\alpha_1 = \alpha_2$, then $\bar{\mathbf{I}}$ is isotropic (e.g., constant) and thus there is no predominant gradient. With structure tensors we acquire robust estimation of gradient orientations in the presence of noise, mainly due to the Gaussian filtering of gradients.

With reference to Fig. 4, we define $g(\mathbf{p}, \mathbf{a})$ as the angle $\theta_{\mathbf{p}, \mathbf{a}} \in [0, \pi]$ between the predominant gradient orientation $\mathbf{v}_1^{\mathbf{p}}$ of \mathbf{p} and a candidate line \mathbf{a} . Denoting the normalized direction of \mathbf{a} as \mathbf{v}_a , we have

$$g(\mathbf{p}, \mathbf{a}) = \theta_{\mathbf{p}, \mathbf{a}} = \cos^{-1} \langle \mathbf{v}_1^{\mathbf{p}}, \mathbf{v}_a \rangle. \quad (3)$$

For point \mathbf{q} , the feature $g(\mathbf{q}, \mathbf{a})$ is computed analogously.

Similarity between $g(\mathbf{p}, \mathbf{a})$ and $g(\mathbf{q}, \mathbf{a})$ is measured by a boxcar function $\delta_\tau(|g(\mathbf{p}, \mathbf{a}) - g(\mathbf{q}, \mathbf{a})|)$, allowing us to exclude point pairs that are not close to being symmetric. It is 1 if its argument is less than τ , and 0 otherwise. The threshold $\tau > 0$ is introduced to improve tolerance to noise. We found that

$\tau = 0.1$ is a reasonable trade off between resistance to noise and not excluding too many points for accurate estimation.

The above similarity measure may be applied to all pixels in a micro-image, leading to the following objective function to estimate the axis of symmetry $\hat{\mathbf{a}}$ over all possible candidate lines \mathbf{a} :

$$\hat{\mathbf{a}} = \arg \max_{\mathbf{a}} \sum_{\{\mathbf{p}\}} \delta_{\tau}(|g(\mathbf{p}, \mathbf{a}) - g(\mathbf{q}, \mathbf{a})|) \quad (4)$$

s.t. $d(\mathbf{c}_s, \mathbf{a}) \leq t$,

where $\{\mathbf{p}\}$ is the set of pixels in the micro-image. We empirically set $t = 10$ for a good balance between the accurate estimation and tolerance to noise.

Optimizing the objective function of (4) can be time consuming. To significantly reduce the computational complexity, two refinements are applied to the above optimization. First, we sample N candidate lines $\{\mathbf{a}_n\}_{n=1}^N$ to be considered in the maximization objective for each micro-image ($N = 5$ in our experiments). Candidates are selected based on the fact that the optical center lies on a line that passes through the micro-image center and the brightest point in the micro-image. In the absence of noise and the attenuation by vignetting, the latter would be the image of the main lens center through the corresponding microlens. This point is likely located at sub-pixel coordinates. Hence, we sample several candidate lines that go through the micro-image center and points around the brightest pixel in the micro-image. The lines are chosen such that they satisfy the constraint $d(\mathbf{c}_s, \mathbf{a}) \leq t$.

For each candidate \mathbf{a}_n , we then estimate the number of symmetric corresponding point pairs. These pairs are chosen in an efficient manner as follows. For each pixel \mathbf{p} on the one side of \mathbf{a}_n , we compute the corresponding point \mathbf{q} on the other side. If \mathbf{q} is at a sub-pixel location, we interpolate the intensity at \mathbf{q} and the pixel patch around it by bilinear interpolation, a simple yet effective method which exploits the local smoothness of the white image. Finally, we select the line that leads to the maximum number of symmetric point pairs as the solution to (4).

B. Optical Center Estimation

The second step of the algorithm estimates the optical center $\mathbf{c}_o = (c_{o,1}, c_{o,2})$ by computing the intersection of the K detected symmetry axes. Collecting all axes into a $K \times 3$ matrix \mathbf{A} with elements $\hat{a}_{k,i}$ and rows $\hat{\mathbf{a}}_k$. Due to the presence of both pixel quantization and noise, detected symmetry axes are unlikely to have one common intersection point. Instead, we determine the optical center by minimizing the sum of distances \mathcal{C} between \mathbf{c}_o and each symmetry axis $\hat{\mathbf{a}}_k$:

$$\mathcal{C} = \sum_k \frac{|\hat{\mathbf{a}}_k \cdot (c_{o,1}, c_{o,2}, 1)^T|}{\|\hat{\mathbf{a}}_k\|_2}. \quad (5)$$

In practice, it is difficult to minimize \mathcal{C} due to the presence of absolute values. Instead, we minimize the following sum of squared distances:

$$\mathcal{C}^* = \sum_k \left(\frac{\hat{\mathbf{a}}_k \cdot (c_{o,1}, c_{o,2}, 1)^T}{\|\hat{\mathbf{a}}_k\|_2} \right)^2. \quad (6)$$

z.s.	982		860		360	
f	6	7	8	9	24	25
e	1.53	1.64	1.28	1.39	0.29	0.34

TABLE I
ERROR e OF ESTIMATED OPTICAL CENTER (IN PIXELS) FOR THE LYTRO CAMERA. THE ERROR IS MEASURED AS FUNCTION OF ZOOM STEP Z.S. AS WELL AS FOCAL LENGTH f (IN MM).

F	2.8	3.4	4	4.8	5.6	6.8	8
e	2.68	3.07	3.27	4.20	4.68	4.84	5.48

TABLE II
ERROR e OF THE ESTIMATED OPTICAL CENTER (IN PIXELS) FOR THE RAYTRIX CAMERA. THE ERROR IS MEASURED AS FUNCTION OF THE f -NUMBER.

This is achieved by setting the partial derivatives of \mathcal{C}^* w.r.t. $c_{o,1}$ and $c_{o,2}$ to 0, which results in the following estimation of the optical center $\hat{\mathbf{c}}_o$:

$$\hat{\mathbf{c}}_o = \begin{bmatrix} \sum_k \frac{\hat{a}_{k,1}^2}{w_k} & \sum_k \frac{\hat{a}_{k,1} \hat{a}_{k,2}}{w_k} \\ \sum_k \frac{\hat{a}_{k,2} \hat{a}_{k,1}}{w_k} & \sum_k \frac{\hat{a}_{k,2}^2}{w_k} \end{bmatrix}^{-1} \begin{bmatrix} -\sum_k \frac{\hat{a}_{k,1} \hat{a}_{k,3}}{w_k} \\ -\sum_k \frac{\hat{a}_{k,2} \hat{a}_{k,3}}{w_k} \end{bmatrix} \quad (7)$$

where $w_k = \|\hat{\mathbf{a}}_k\|_2^2$. The estimated optical center $\hat{\mathbf{c}}_o$ can then be used for image modeling and post-processing applications.

IV. RESULTS

We first validate the accuracy of the proposed optical center estimation on simulated plenoptic images and then apply the algorithm to real data.

A. Simulated Data

The intrinsic accuracy of our algorithm is asserted with the aid of synthetic data, giving us access to the ground truth. We synthesize white images from the light field model in [6], and using a range of focal lengths of $f \in \{3, 5, 7, 9\}$ mm, assuming a Lytro lens system. The synthesized white images are 820×820 in pixels, with the ground truth optical center set as $(410, 410)$. For each white image, we normalize pixel intensities to $[0, 1]$, and add white Gaussian noise with varying noise levels (standard deviations $\sigma_n \in \{0.02, 0.1, 0.5, 1\}$) to simulate sensor noise, as illustrated in Fig. 5. For each noise level 16 realizations are generated for each focal length to measure the statistics of the estimation error.

The estimation error is shown in Fig. 6. Gaussian noise with $\sigma_n = 0.02$ is close to most sensor noise observed from captured plenoptic data. For such noise level, the average estimation error is 0.26 pixels for $f = 3$ mm, 0.32 pixels for $f = 5$ mm, 0.37 pixels for $f = 7$ mm and 0.38 pixels for $f = 9$ mm. Higher values of simulated sensor noise yield larger estimation errors, but Fig. 6 shows that even for extreme noise levels, the estimation error mostly remains less than half a pixel, validating the accuracy and robustness of our algorithm. Further, we observe that the estimation error

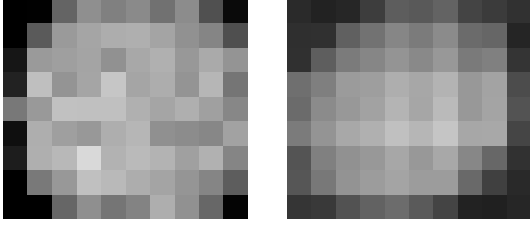


Fig. 5. One micro-image in the synthesized white image with $f = 8$ mm and added Gaussian noise with $\sigma_n = 0.1$ (left), and one micro-image in a white image captured by Lytro after demosaicking (right).

increases for longer focal lengths, due to less pronounced vignetting.

We observe that the nature of the vignetting in plenoptic cameras enables us to design a calibration algorithm that is one to two orders of magnitude more accurate than what can currently be obtained for conventional cameras. Compare, for instance, the accuracy range of 1 to 15 pixels obtained for conventional images [9]. Note that this method cannot be applied to plenoptic data for direct comparison, as that method is designed for conventional images lacking the micro-image patterns in raw data.

Finally, the results of the optical center estimation are obtained from synthetic data, where the (possibly imperfect) estimation of the microlens centers is performed according to [20], [21]. These results are then compared with the ground truth data. Our optical center estimation has shown to perform well despite the fact that the micro-center image estimation by [20], [21] might be biased.

B. Real Data

We apply our algorithm to the analysis of the first generation Lytro camera and the Raytrix camera. The dimensions of the stored white images for the Lytro are 3280×3280 pixels. For Raytrix we capture white images of 2046×2046 pixels placing a white diffuser in front of the main lens. Each individual micro-image is extracted by estimating its center [20], [21], accounting for micro-lens array misalignment [20], and then taking an $r \times r$ patch centered at the corresponding micro-image center ($r = 10$ for Lytro and $r = 17$ for Raytrix according to the camera parameters).

Tables I and II show the Euclidean distances e between the estimated optical centers and the center of the sensor plane for Lytro and Raytrix respectively. For the Lytro camera, both zoom step (an indication of the amount of the applied optical zoom) and focal length were varied. For the raytrix camera, the F -number was varied. All the other parameters remained fixed.

With the camera settings mentioned in Tables I and II, the deviation of the estimated optical center from the sensor center was found to be on average 1.08 pixels, with the standard deviation of 0.6 pixels and the maximum of 1.64 pixels for Lytro cameras. The optical center displacement from the sensor center had an average of 4.03 pixels, a

standard deviation of 1.04 pixels and the maximum of 5.48 pixels for Raytrix cameras, dependent on camera settings. This indicates that the manufacturing precision of optical systems is amenable to improvement. At the same time, as the deviation of the optical center affects image formation, it should be taken into consideration for post-processing applications.

V. APPLICATIONS

In the following, we show two applications which can benefit from the use of our work, namely plenoptic camera calibration, and the correction of vignetting.

A. Plenoptic Camera Calibration

To demonstrate the impact of an accurate optical center estimation, we optimize the two most uncertain parameters—the focal length f and the angular sensitivity parameter σ in the remaining intrinsic camera parameters in [6] by minimizing the squared error between a captured white image and its modeled counterpart.

We first generate 820×820 pixel input white images, varying the optical center and focal length for evaluation. The set of the main-lens focal lengths f is $\{3, 5, 7, 9\}$ mm, and optical center is shifted both horizontally and vertically from the image center by $\delta_{x,y} \in \{5, 25, 50, 100\}$ pixels. As the shift of the optical center is experimentally varied over a large range, we set the threshold t in (4) to $1.5 \delta_{x,y}$ accordingly. The white images are synthesized using an angular sensitivity σ set to 13 [6]. Further, Gaussian noise with a standard deviation of 0.02 is added to mimic sensor noise.

We estimate f and σ by fitting the model in [6]

to these synthesized white images. This is achieved by applying non-linear least-squares curve fitting. For comparison, we use two types of initialization: 1) with the image center as the optical center; 2) with our estimated optical center.

Fig. 7 shows the percentage of the estimation error for f and σ respectively. The error grows more or less linearly if the center of the sensor is assumed to be equal to the optical center. It is clear that with our estimated optical center as initialization, the error percentage effectively remains constant, independent of how far the optical center deviates from the center of the sensor.

B. Vignetting Correction

As an example of the practical benefit of our method, we use the model in [6], with and without our estimated optical center, to correct for vignetting. To this end, we use our estimated optical center to aid in the synthesis of white images using the model in [6]. We then divide an input white image with vignetting by these synthesized white images, obtaining a corrected image. Fig. 8 shows the results on a single representative micro-image for clear illustration. Note that the improved accuracy of the optical center leads to a significantly better correction, effectively eliminating vignetting entirely.

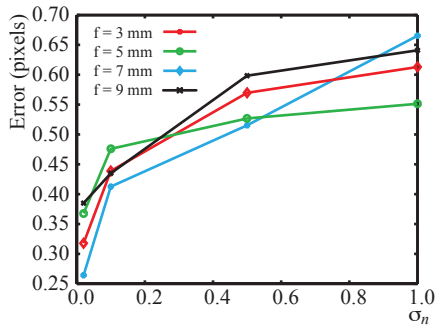


Fig. 6. Estimation error using synthetic data with additive white Gaussian noise σ_n .

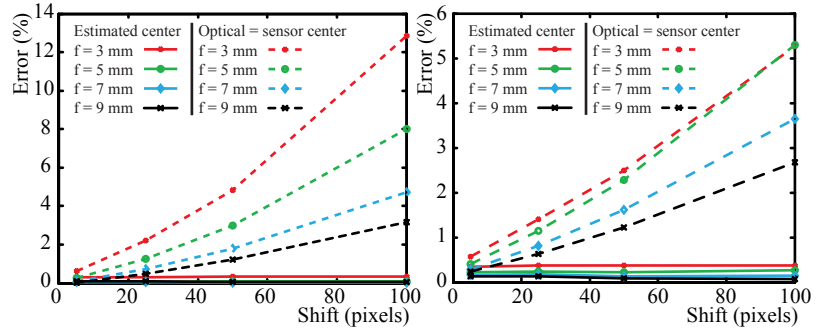


Fig. 7. Different initialization of the optical center leads to different optimized parameters including (left) the focal length of the main lens, and (right) the angular sensitivity.

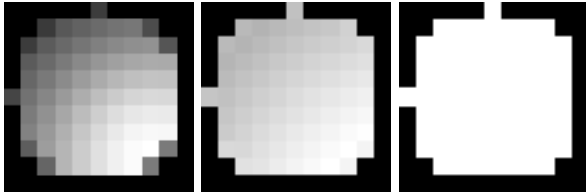


Fig. 8. The synthesized input white image (left), its corrected version. For the middle image, the vignetting model was optimized by setting the optical center to the image center. The right image was created by estimating the optical center using our algorithm.

VI. CONCLUSIONS

We propose a robust and accurate optical center estimation for plenoptic cameras. The key idea is to exploit the reflection symmetry of micro-images captured from a uniform scene, knowing that the symmetry axes of each micro-image should intersect at the optical center. The accuracy of our algorithm is verified first on a realistic number of experiments using synthetic data showing an estimation error of less than half a pixel on average at various noise levels. We have also demonstrated the utility of this method in the context of camera calibration and vignetting correction. In the future, there may be value in expanding the method to work with captured images of other stimuli than monochrome signal.

VII. ACKNOWLEDGEMENT

This work has been supported by National Natural Science Foundation of China under contract No. U1636206.

REFERENCES

- [1] R. Ng, M. Levoy, B. Mathieu, G. Duval, M. Horowitz, and P. Hanrahan, "Light field photography with a hand-held plenoptic camera," in *Computer Science Technical Report CSTR*, 2005.
- [2] M. Tao, S. Hadap, J. Malik, and R. Ramamoorthi, "Depth from combining defocus and correspondence using light-field cameras," in *International Conference on Computer Vision*, Sydney, 2013, pp. 673–680.
- [3] C. Perwass and L. Wietzke, "Single lens 3d-camera with extended depth-of-field," in *Proceedings of SPIE Electronic Imaging*, 2012, pp. 829 108–829 108.
- [4] A. Vetro, T. Wiengand, and G. Sullivan, "Overview of the stereo and multiview video coding extensions of the H.264/MPEG-4 AVC standard," in *Proceedings of the IEEE*, vol. 99, no. 4, 2011, pp. 626–642.
- [5] A. Hinds, D. Doyen, and G. Lafruit, "Call for light field test material including plenoptic cameras and camera arrays," Internet draft : mpeg.chiariglione.org/standards/exploration/immersive-video/, 2016.
- [6] C. K. Liang and R. Ramamoorthi, "A light transport framework for lenslet light field cameras," in *ACM Transactions on Graphics*, vol. 34, no. 2, 2015, pp. 16:1–16:19.
- [7] Y. Zheng, S. Lin, C. Kambhmettu, J. Yu, and S. B. Kang, "Single-image vignetting correction," in *IEEE Transactions on Pattern Analysis and Machine Intelligence*, vol. 31, no.12, 2008, pp. 2243–2256.
- [8] Z. Xue, L. Baboulaz, P. Prandoni, and M. Vetterli, "Light field panorama by a plenoptic camera," in *IS&T/SPIE Electronic Imaging*. International Society for Optics and Photonics, 2014, pp. 90 200S–90 200S.
- [9] Y. Zheng, C. Kambhmettu, and S. Lin, "Single-image optical center estimation from vignetting and tangential gradient symmetry," in *IEEE Conference on Computer Vision and Pattern Recognition*, 2009.
- [10] R. I. Hartley, E. Hayman, L. D. Agapito, and I. Reid, "Camera calibration and the search for infinity," in *International Conference on Computer Vision*, 1999, pp. 510–517.
- [11] S. Kang and R. Weiss, "Can we calibrate a camera using an image of a flat textureless lambertian surface?" in *European Conference on Computer Vision*, 2000, pp. 640–653.
- [12] D. G. Dansereau, O. Pizarro, and S. B. Williams, "Decoding, calibration and rectification for lenselet-based plenoptic cameras," 2013.
- [13] R. G. Willson, "Modeling and calibration of automated zoom lenses," in *Photonics for Industrial Applications*. International Society for Optics and Photonics, 1994, pp. 170–186.
- [14] C. Sun and D. S., "Fast reflectional symmetry detection using orientation histograms," *Real-Time Imaging*, vol. 5, no. 1, pp. 63–74, 1999.
- [15] T. Yuan and X. Tang, "Efficient local reflectional symmetries detection," in *IEEE International Conference on Image Processing*, vol. 3, 2005, pp. III–1180.
- [16] S. Tsogkas and I. Kokkinos, "Learning-based symmetry detection in natural images," in *European Conference on Computer Vision*. Springer, 2012, pp. 41–54.
- [17] U. Köthe, "Edge and junction detection with an improved structure tensor," in *Joint Pattern Recognition Symposium*. Springer, 2003, pp. 25–32.
- [18] H. Li, P. J. Olver, and G. S. (Eds.), *Computer Algebra and Geometric Algebra with Applications*. Berlin: Springer-Verlag, 2005, vol. 3519.
- [19] H. S. Malvar, L. W. He, and R. Cutler, "High-quality linear interpolation for demosaicing of bayer-patterned color images," in *International Conference of Acoustic, Speech and Signal Processing*, Montreal, 2004, pp. iii–485.
- [20] N. Sabater, S. M., V. Drazic, G. Sandri, and P. Pérez, "Accurate disparity estimation for plenoptic images," in *European Conference on Computer Vision*, Zurich, 2014, pp. 548–560.
- [21] M. Hog, N. Sabater, B. Vandame, and V. Drazic, "An image rendering pipeline for focused plenoptic cameras," hal-01401501, 2016.